Nuclear-structure studies of exotic nuclei with MINIBALL

OPEN ACCESS
IOP Publishing

Made open access 12 September 2017
Journal of Physics G: Nuclear and Particle Physics

J. Phys. G: Nucl. Part. Phys. **44** (2017) 044012 (23pp) https://doi.org/10.1088/1361-6471/aa5c4e

Nuclear-structure studies of exotic nuclei with MINIBALL

P A Butler[1], J Cederkall[2] and P Reiter[3]

[1] Oliver Lodge Laboratory, University of Liverpool, Liverpool L69 7ZE, United Kingdom
[2] Physics Department, University of Lund, Box 118, SE-221 00 Lund, Sweden
[3] Institute of Nuclear Physics, University of Cologne, D-50397 Cologne, Germany

E-mail: preiter@ikp.uni-koeln.de

Received 16 November 2016, revised 24 January 2017
Accepted for publication 26 January 2017
Published 9 March 2017

Abstract

High-resolution γ-ray spectroscopy has been established at ISOLDE for nuclear-structure and nuclear-reaction studies with reaccelerated radioactive ion beams provided by the REX-ISOLDE facility. The MINIBALL spectrometer comprises 24 six-fold segmented, encapsulated high-purity germanium crystals. It was specially designed for highest γ-ray detection efficiency which is advantageous for low-intensity radioactive ion beams. The MINIBALL array has been used in numerous Coulomb-excitation and transfer-reaction experiments with exotic ion beams of energies up to 3 MeV A^{-1}. The physics case covers a wide range of topics which are addressed with beams ranging from neutron-rich magnesium isotopes up to heavy radium isotopes. In the future the HIE-ISOLDE will allow the in-beam γ-ray spectroscopy program to proceed with higher secondary-beam intensity, higher beam energy and better beam quality.

Keywords: nuclear structure, γ-ray spectroscopy, shell model, nuclear shapes

(Some figures may appear in colour only in the online journal)

1. Introduction

Studies using low-energy beams of short-lived radioactive nuclei has been the main field of activity in the ISOLDE collaboration. In order to study the properties of radioactive nuclei by reactions at moderate beam energies employing Coulomb excitation and transfer reactions, the Radioactive beam EXperiment at ISOLDE (REX-ISOLDE) was proposed in 1994 [1, 2] and became operational in 2001. The post-accelerator relied upon the production of highly-charged ions which ensured the installation of a compact, efficient and cost-effective

experimental setup. Singly-charged radioactive ions coming from ISOLDE are first cooled and bunched in a Penning trap (REXTRAP) [3] before they are charge bred to higher charge states, using an electron-beam ion source (REXEBIS) [4, 5]. The ions with a mass-to-charge ratio of $A/q < 4.5$ are post-accelerated in a compact linear accelerator (REX-LINAC) and delivered to the experimental area. The complete facility is described in detail in [6–8]. REX-ISOLDE was originally designed for post-acceleration of neutron-rich light isotopes. However, the novel acceleration scheme, especially the charge breeding technique, was very versatile; it could be extended to heavier ions. More than 90 different radioactive isotopes, ranging from the light ^{8}Li up to the heavy actinide isotope ^{224}Rn have been efficiently post-accelerated by REX-ISOLDE up to energies of 3.0 MeV/A before the long shut-down period started at CERN in 2013.

Already the initial REX-ISOLDE proposal [9] suggested a novel position sensitive γ-ray spectrometer as the main instrument to study de-excitation γ rays following the induced nuclear processes. Several technical demands had to be met by this detector array. The low beam intensities are low so that the spectrometer has to be highly efficient. The isotopes of interest are radioactive, creating a large amount of background radiation. Therefore high-resolution detectors are needed in order to maximize the peak-to-background ratio. Scattered nuclei recoil at high velocities of typically 5%–10% of the speed of light causing significant Doppler shifts and broadening. To maintain the very good energy resolution, position sensitivity or a high granularity is necessary, in order to obtain a sufficient small effective opening angle of the detector in a compact configuration. All these requirements influenced the design of the MINIBALL detector array.

The initial physics program suggested by the proposal for the MINIBALL at REX-ISOLDE started with a thorough investigation of neutron-rich Na and Mg nuclei in the vicinity of the $N = 20$ shell by means of Coulomb excitation (CE) and neutron-transfer reactions [10–15]. Simultaneously experiments along the chains of neutron-rich Ni, Cu and Zn isotopes were pursued in order to study collective and single particle properties in the vicinity of $N = 40$ and the doubly-magic configuration at ^{78}Ni [16–28]. Moreover, the first g-factor measurement of excited states was successfully performed with a radioactive ion beam at ISOLDE in this region [24]. A shell-model study was dedicated to the neutron deficient Sn isotopes, where unexpected high values for CE of the first excited 2_1^+ state were observed [29–35]. Isotopes around the doubly-magic nucleus ^{132}Sn were subject of CE experiment [36].

The extended REX-ISOLDE acceleration scheme was readily applied to even heavier ions and enabled detailed studies of shapes and collectivity in very neutron-rich and neutron-deficient Se, Kr, Rb and Sr nuclei [37–42] as well in the rare-earth region [43–45]. In recent years results for neutron-deficient Hg, Pb, Po, Rn isotopes were also obtained from CE experiments which provided valuable and complementary insights to the understanding of the structure of this mass region to that obtained using heavy-ion induced fusion reactions [46–48]. The heaviest nuclei, which were accelerated by REX-ISOLDE and investigated by MINIBALL, were the actinide isotopes ^{220}Rn and ^{224}Ra. For these nuclei intriguing results related to dynamic and static octupole deformation were obtained [49]. A first review article on the reacceleration of radioactive beams at REX-ISOLDE, the instrumentation and the experimental techniques and the MINIBALL physics program was published in 2011 [50]; a recent comprehensive description of the MINIBALL spectrometer and its operation at REX-ISOLDE was given in [51].

This review will start with a description of the MINIBALL spectrometer and its ancillary detectors. The physics program is illustrated by selected studies of the Na and Mg isotopes at the island of inversion, the region around neutron-rich Ni isotopes between $N = 40$ and

$N = 50$ and the neutron-deficient Sn isotopes. Examples of measurements of shape coexistence in atomic nuclei are given for $N \approx Z$ nuclei near ^{72}Kr, neutron rich Kr, Sr, Zr near $N = 60$ and the neutron-deficient Hg, Po, Rn region. This is followed by an example of an octupole deformed nuclei with $A \approx 200$.

2. MINIBALL spectrometer

2.1. γ-ray array

Due to the requirements needed for low-intensity radioactive ion-beam experiments at significant recoil velocities the MINIBALL array was developed to obtain high-energy resolution and high detection efficiency for nuclear reactions with low γ-ray multiplicity events. The γ-ray spectrometer is built of large volume n-type high-purity germanium (HPGe) crystals (length 78 mm, diameter 70 mm) which are individually encapsulated. The outer contact of the hexagonal shaped crystal is electronically six-fold segmented. Three of these crystals are assembled together in a common cryostat forming a triple-cluster detector. Eight triple-cluster detectors are installed on arc-shaped arms which allow a flexible mounting of the HPGe detectors around the target chamber. In most cases a high solid-angle coverage is accomplished in a compact configuration. With the optimum distance between target chamber and Ge-detectors, the array covers a solid angle of about 60% of 4π. Due to its flexibility special requirements of detector configurations are easily accommodated e.g. for measurements of angular correlations, nuclear g-factors or lifetimes.

Front-end signal processing of the 168 individual signals from the central core electrodes and segment contacts is based on broad-band preamplifiers with cold FET technology and digital electronics, enabling count rates of up to 20 kHz per detector. An average energy resolution of 2.3 keV at $E = 1.3$ MeV is achieved. The photopeak efficiency of MINIBALL is about 8% at this γ-ray energy for the compact configuration. The electrical segmentation of the outer detector contact increases the granularity and thus reduces the effective solid angle for the individual γ-ray. In this way large Doppler shifts and broadening are corrected effectively for in-flight γ-ray emission at high velocities even at the very close distances between target and detector. In addition pulse shape analysis of all detector signals is possible. This allows the first interaction point of the γ-ray to be defined in order to improve the position resolution. The combined information from the charge collection at the central electrode and at the segments gives the interaction point of the γ ray in radial and azimuthal direction. A two dimensional position resolution of about 7.5 mm (FWHM) is obtained with the segmented MINIBALL HPGe detectors. A detailed description of the spectrometer is provided by [51–54]. A picture of the spectrometer and its surrounding infrastructure is shown in figure 1.

2.2. Particle detectors

To ensure a proper Doppler correction for in-flight γ-ray emission at high velocities, the angular information of the γ ray, provided by the position-sensitive MINIBALL detectors, is combined with the direction and velocity of the scattered beam particle that was measured in coincidence. For this purpose the scattered beam and recoiling target nuclei are detected by silicon strip detectors which are employed in two different configurations for identification and reconstruction of the trajectories of the scattered nuclei. First, a CD-shaped double-sided silicon strip detector (DSSSD) is typically used for CE experiments in order to detect forward-scattered beam- or target-like reaction products. This device consists of four identical

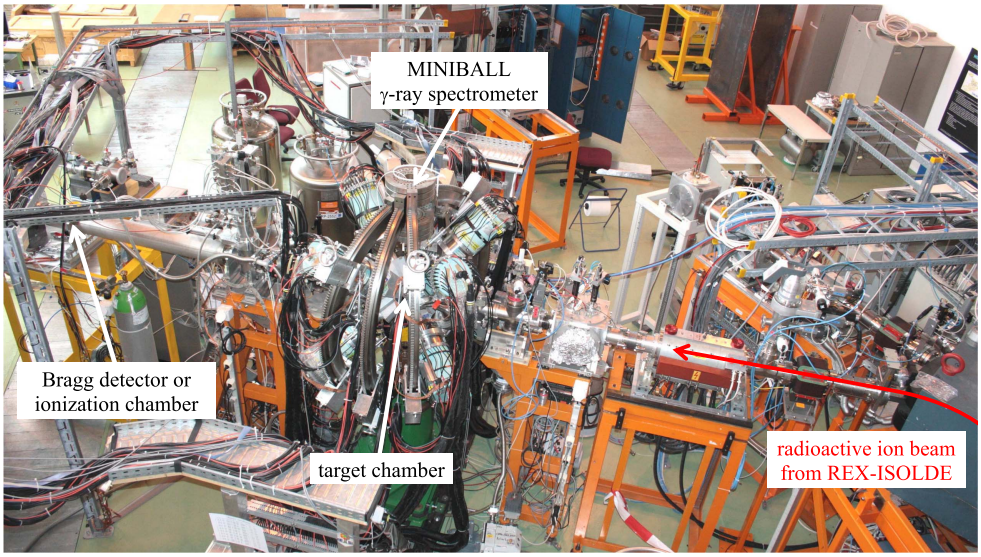

Figure 1. Picture of the MINIBALL setup in 2010. The radioactive ion beam delivered by REX-ISOLDE is coming from the bottom right, hitting the secondary target right in the middle of the MINIBALL spectrometer. Downstream of the scattering chamber additional detector systems are installed to monitor the position of the beam and its composition.

quadrants with different Si wafer thicknesses between 35 and 500 μm. Each quadrant is highly segmented by 16 annular strips of 2 mm pitch at the front side and by 24 radial strips of 3.5° pitch at the back side. The detector geometry covers the angular range between 16° and 54° under forward direction [55].

A second particle detector array was realized later in 2007 in order to extend the physics program at REX-ISOLDE to transfer reactions in inverse kinematics. The T-REX target chamber was designed and was built for maximum efficacy for both particle and γ-ray detection. The T-REX array consists of two CD-shaped 500 μm DSSSDs, one in forward and one in backward direction, and a barrel of eight position-sensitive planar detectors, positioned symmetrically around 90°. Both the forward and backward DSSSDs are stacked with 500 μm unsegmented E-detectors in order to form $\Delta E - E$ telescopes for identification of different reaction products. These can be the different light ejectiles from the target (p, d, t, α) and heavier isotopes, such as beam-like particles or the heavy carrier material of the target in forward direction. The forward and backward barrel detectors are identical and consist of a stack of 140 and 1000 μm planar Si detectors. The thinner Si detectors are segmented in 16 strips perpendicular to the beam axis. Position information along these strips is obtained from the charge division on a resistive layer. The thicker Si detectors are not segmented. This stack of Si detectors serves also as a $\Delta E - E$ telescope to identify the different ejectiles from the target. All detectors are protected by foils, which stops beam particles scattered off the target. The energy resolution for light particles ranges typically from 250 keV to 2 MeV, depending on their scattering angle, energy and the target thickness. Therefore, it is crucial to detect coincident γ rays, which are used to identify the populated final state with the much higher HPGe-detector resolution. By gating on a γ ray which depopulates the state, it is possible to deduce the angular distribution of the emitted protons which correspond to the excitation of that state. The angular resolution of the particle detector is typically better than 5° [56, 57].

2.3. Ancillary detectors and time structure of the RIB

A position-sensitive parallel plate avalanche counter can be placed on the beam axis behind the target for measurement of the beam profile perpendicular to the beam direction. It consists of a central anode foil and two segmented cathode foils, mounted inside a gas volume. Both cathode foils are segmented to allow a position sensitive readout of the particle flux in both directions.

Close to the beam dump position a Bragg ionization chamber is mounted, to allow a permanent monitoring of the beam composition in mass and charge. A homogeneous electrical field can be applied along the gas volume on 20 electrodes. The incoming ions loose their energy in the gas, following the characteristic energy loss curve of the Bethe-Bloch formula. Due to the applied electrical field the generated charges drift with a constant velocity towards the anode. From the time evolution of the anode pulse the mass A and charge Z of the incoming particle is deduced.

The device that is commonly used to continuously survey the RIB composition is a $\Delta E - E_{\mathrm{Res}}$ detector. It consists of a gas-filled ionization chamber with CF_4 at a pressure of 300–450 mbar, generating a charge Z dependent energy loss ΔE signal, coupled to a silicon detector for the measurement of the residual energy E_{Res}. As all ions have the same energy per nucleon, the mass A can be derived from E_{Res}. An adjustable collimator is put in front of the entrance windows of the ionization chamber to attenuate the incoming beam intensity in order to prevent pile-up.

The radioactive ion beam provided by REX-ISOLDE is not a continuous flux of particles, but it is delivered in short particle bunches with a characteristic time structure. It is caused by the time-dependent yield of the ions of interest due to their release and radioactive decay and by the duty cycles of the charge-breeding and accelerating systems. While the small duty cycle can aggravate the effect of background arising from pile-up and random coincidences, in-beam spectroscopy experiments can benefit from this feature by efficient background suppression. In order to synchronize the data acquisition at the MINIBALL setup with the production and acceleration of the radioactive ions, different time signals are exploited at ISOLDE. The first periodic time signal is the time pulse at the beginning of each super cycle of the CERN PS Booster (PSB). This time signal is especially relevant for experiments with laser ion sources, to drive a shutter which periodically blocks the laser light towards the ionization tube. The analysis of the nuclear reaction events can be limited to a time window which combines various conditions, e.g. (1) the time difference of a few half-lifes of the ions of interest with respect to the signal of proton beam impact can be selected; (2) there can be a requirement that the shutter of the laser ion source is open, allowing the element of interest to be selected; (3) a time window can be employed which signals that the charge bred ions are injected from the EBIS into the accelerator. In this way background from long-lived or stable contaminants can be strongly suppressed.

3. Magic nuclei and the evolution of nuclear shells

3.1. The island of inversion

The exotic neutron-rich nuclei at $N = 20$ are up to now one of the prime examples where unexpected sudden changes of nuclear properties, associated with the traditional landmarks of nuclear structure, occur. For these nuclei it has been realized that the interaction of the last valence protons and neutrons, in particular the monopole component of the residual interaction between those nucleons, can lead to significant shifts in the single-particle energies,

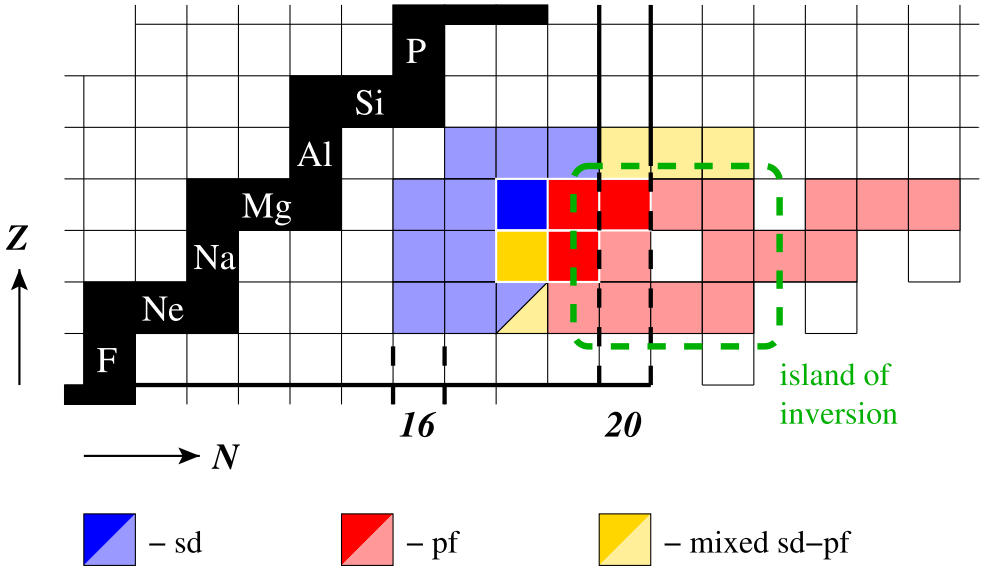

Figure 2. Detail of the Segrè chart showing the region of the island of inversion. The isotopes ^{30,31,32}Mg and ^{29,30}Na were investigated at REX-ISOLDE by means of safe CE and transfer reactions. The transition between normal *sd* ground-state configuration and the intruder *pf* configuration is delineated. Results for the more neutron-rich isotopes were obtained in recent years; the isotopes that have been examined are marked for completeness. For further information see text.

leading to the collapse of classic shell closures and the appearance of new shell gaps. The island of inversion around ^{32}Mg, with neutron-rich nuclei at and close to the magic number $N = 20$ (illustrated in figure 2) shows strongly deformed ground states in Ne, Na, and Mg isotopes. This is related to the reduction of the $N = 20$ shell gap and quadrupole correlations enabling low-lying deformed $2p2h$ intruder states from the higher *fp* shell to compete with spherical normal neutron $0p0h$ states of the *sd*-shell. The promotion of a neutron pair across the $N = 20$ gap can result in deformed intruder ground states and the two competing configurations can lead to the coexistence of spherical and deformed 0^+ states in the neutron rich nuclei ^{30,32}Mg.

The first convincing indication for the low-lying intruder states was deduced from the 2^+ state measured in RIKEN in 1995 for ^{32}Mg using the new technique of intermediate-energy CE [58]. A large $B(E2)$ value of $454(78)e^2fm^4$ was measured corresponding to a large quadrupole deformation of the ground state. These findings were exceeding expectations for a semi-magic nucleus. Later on the $B(E2)$ values for the neutron-rich Mg isotopes ^{30,32,34}Mg were measured by different groups at the intermediate-energy facilities MSU [59, 60] and GANIL [61] showing a wide range of results (see figure 3).

In order to clarify the situation a spectroscopic program with MINIBALL was started in 2003 and transition-strength values in ^{30,31,32}Mg and in ^{29,30}Na were determined employing the complementary technique of sub-barrier CE in inverse kinematics at safe energies. In comparison with the intermediate-energy CE, the new approach gave improved γ-ray energy resolution and cleaner background conditions. The results are barely influenced by nuclear interference effects and by excitations of higher-lying states. The Radioactive beam EXperiment for the post-acceleration of radioactive beams was ideally suited for this purpose.

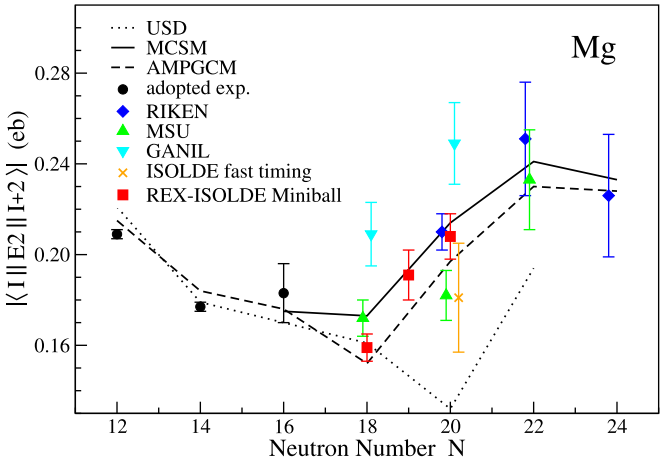

Figure 3. $E2$ transitional matrix elements for the chain of neutron-rich Mg isotopes from $N = 12$–24. Additionally, the $E2$ transition matrix element for the $1/2_1^+ \rightarrow 5/2_1^+$ excitation from the ground state in ^{31}Mg was measured with MINIBALL at REX-ISOLDE. This value corroborates the findings from the ground-state configuration with its intruder configuration. The given values comprise results from experiments performed at RIKEN [58, 62], MSU [59, 60], GANIL [59, 60] and at ISOLDE employing safe CE [11, 13, 63] and the fast-timing technique after β decay [64]. While for $N \leqslant 18$ the experimental values are well reproduced by USD shell-model calculations [65], large deviations are found for $N \geqslant 20$. Dominant $2p2h$ configurations were taken into account for the ground state of ^{32,34,36}Mg by Monte-Carlo Shell Model (MCSM) calculations [66] and beyond-mean-field calculations (AMPGCM) [67].

The maximum beam energy was up to 3.0 MeV/A at this time. De-excitation γ rays were detected by the MINIBALL spectrometer in coincidence with scattered particles in the CD shaped segmented Si-detector under forward direction.

The CE experiments have proven that the deformed $sd - pf$ intruder configuration is dominating the ground state of ^{32}Mg [63]. In contrast a much reduced excitation of $B(E2) = 280(20)e^2fm^4$ for the 2^+ state at 1483 keV was found in the $N = 18$ isotope ^{30}Mg [11], which is consistent with a spherical ground state configuration. The clear experimental results from the two even–even isotopes ^{30,32}Mg inspired a detailed investigation of the unstable odd-N nucleus ^{31}Mg. The ground state properties of ^{31}Mg indicated already a change of nuclear shape at $N = 19$ with a deformed $J^\pi = 1/2^+$ intruder state as a ground state, implying that ^{31}Mg is part of the island of inversion [68].

Therefore, the collective properties of excited states in ^{31}Mg were examined by means of CE. The level scheme of ^{31}Mg was extended. Spin and parity assignment of a new state at 945 keV yielded $5/2^+$ and its de-excitation is dominated by a strong collective M1 transition. The properties of a positive-parity yrast band with $K = 1/2$, built on the $1/2^+$ ground state, are in good agreement with the $5/2^+$ state at 945 keV. The measured $B(E2)$ and $B(M1)$ values support this assumption. The increased collectivity is well described by the deformed Nilsson model for excited states in ^{31}Mg. Finally, the quadrupole moment supports the idea that for the $N = 19$ magnesium isotope not only the ground state but also excited states are no longer dominated by a spherical configuration. Although the $E2$ strength of the $5/2^+ \rightarrow 1/2^+$ transition in ^{31}Mg is smaller it is comparable to the corresponding $2^+ \rightarrow 0^+$ transition in ^{32}Mg. The deviation could be explained by the assumption that higher-lying states in ^{31}Mg

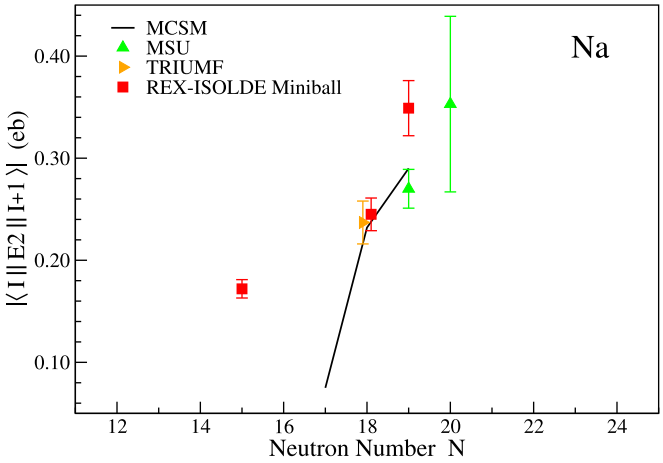

Figure 4. $E2$ transitional matrix elements for the neutron-rich Na isotopes at $N = 15$, 18–20. The transition matrix element for the $2^+ \rightarrow 3^+_1$ excitation in ^{26}Na is taken from [15]. Other results show values from the following ground-state excitations: $3/2^+ \rightarrow (5/2^+_1)$ in ^{29}Na, $2^+_1 \rightarrow (3^+_1)$ in ^{30}Na, $3/2^{(+)} \rightarrow (5/2^+_1)$ in ^{31}Na. The MINIBALL results [14] and the value for ^{29}Na from TRIUMF [69] are based on safe CE. The MSU values for ^{30,31}Na are measured with intermediate-energy CE and are extracted from [70, 71]. Results from shell-model calculations are taken from [72].

are not dominated by pure intruder configurations, but contain an admixture of other particle-hole configurations [13]. The measured $E2$ matrix elements along the Mg isotopic chain is given in figure 3 illustrating the contribution of the safe CE results in comparison with intermediate-energy CE and a complementary fast-timing experiment from ISOLDE by Mach.

Nuclear shell evolution in neighboring neutron-rich Na nuclei at $N = 20$ was studied by determining reduced transition probabilities, in order to map the border of the island of inversion. To this end CE experiments, employing radioactive ^{29,30}Na beams with a final beam energy of 2.85 MeV/A, were performed employing the MINIBALL spectrometer in coincidence with scattered particles. Transition probabilities to excited states were deduced. The measured $B(E2)$ values agree well with shell-model predictions, supporting the idea of a gradual transition in the Na isotopic chain. While in ^{29}Na the ground-state wave function contains significant intruder admixture already at $N = 18$, results for ^{30}Na with $N = 19$ are consistent with an almost pure $2p2h$ deformed ground-state configuration as predicted by the Monte Carlo shell-model (MCSM) calculations using the SDPF-M interaction [72]. For ^{29}Na a mixing of intruder configurations by 42% and 32% is calculated for the wave function of the $3/2^+$ ground state and the first excited $5/2^+_1$ state, respectively. The onset of large intruder admixtures in the ground state wave function was established already for the $N = 18$ isotope [14]. A comparison between experimental results from MSU, TRIUMF and REX ISOLDE and the MCSM calculation is given in figure 4. Figure 4 includes also a recent $E2$ matrix element value extracted from a ground state transition in ^{26}Na, where no intruder configuration is relevant.

The CE experiments described above focused on the intruder states in the island of inversion with configurations consisting of two neutrons excited from the $0d_{3/2}$ and $1s_{1/2}$ orbitals into the $0f_{7/2}$ and $1p_{3/2}$ orbitals across the $N = 20$ shell gap, forming a $2p2h$ state. A complementary MINIBALL experiment provided the first confirmation that also the predicted

coexisting excited state similar to the closed-shell configuration exists. The beam energy at the REX-ISOLDE facility also enabled transfer-reaction experiments to be performed. Therefore, ^{32}Mg was studied by a (t, p) two-neutron transfer reaction in inverse kinematics with a ^{30}Mg beam. This involved the use of a radioactive tritium target in combination with a radioactive heavy-ion beam. Light charged particles emitted from the target were detected and identified by the T-REX particle detector while γ rays were detected by the MINIBALL. The angular distribution of the protons allowed the angular momentum transfer ΔL of the reaction to be determined. The analysis of excitation energies and angular distribution of the protons led to the first observation of the excited shape-coexisting 0_2^+ state in ^{32}Mg at 1058(2) keV. A more detailed description of these results is given in the chapter about nuclear reactions in this special edition volume.

3.2. The Ni region between the N = 40 and N = 50 shell closures

The re-accelerated radioactive ion beams from REX-ISOLDE were of great relevance for nuclear-structure investigations in very neutron-rich isotopes in the vicinity of ^{68}Ni and ^{78}Ni, spanning the range between the shell gaps at neutron numbers $N = 40$ up to $N = 50$. The experimental campaign started out more than ten years ago when first predictions related to the evolution of shell structure where made and the important role of the tensor interaction and three-body forces were awaiting experimental verification.

At this point an experimental program at REX-ISOLDE commenced with a series of ground-breaking CE measurements which established not only a whole series of new transition-strength values but explored in several cases new and unknown states in the most exotic Cu and Zn isotopes. From the experimental point of view two major advances for in-beam γ-ray spectrocopy with ISOL beams were pioneered in this mass region. First, the use of re-accelerated isomeric radioactive ion-beams in Cu isotopes was established. The isomers were selectively extracted from the ion source by the resonant-ionization laser technique. Second, the sophisticated coupling of the efficient REX-TRAP and the REX-EBIS together with the exploitation of different time sequences for isotopes with different lifetimes allowed beams of refractory Fe isotopes to be prepared. In this way a major obstacle and limitation of the ISOL technique was overcome.

Transfer reactions gave access to the direct neighbors of ^{68}Ni at $N = 40$ and ^{79}Zn at $N = 50$ providing an excellent tool to probe the size of the shell gaps and test the single-particle character of unknown neutron orbitals. One of the first g-factor measurements with a radioactive ion beam was successfully performed in ^{72}Zn using the low-velocity transient-field technique [24].

3.2.1. Coulomb excitation of refractory Fe isotopes. At ISOL facilities, which utilize thick primary-production targets, beams of neutron-rich iron isotopes are difficult to obtain due to the long extraction time of these isotopes out of the target matrix. At REX-ISOLDE, exploratory experiments investigated successfully the possibility of producing a post-accelerated beam of neutron-rich iron isotopes following in-trap decay of neutron-rich manganese isotopes, which are available at ISOLDE using the resonance ionization laser ion source. The trapping time of the Penning trap and the charge-breeding time of the EBIS were optimized in order to alter the composition of the beam, which was measured by means of an ionization chamber at the zero-angle position of the MINIBALL array. The production mechanism was established for the first time at REX-ISOLDE with intense and short-lived beams of ^{61,62}Mn isotopes. The new approach opens up possibilities to perform experimental studies on short-lived isotopes which were previously unavailable at the ISOL facilities.

The physics results on the CE of ^{61}Mn and ^{61}Fe yielded transition strengths in both nuclei. The values compare well to large-scale shell-model calculations. However, the $\nu 1g_{9/2}$ orbital has to be included in the valence space since it affects the quadrupole collectivity even at low excitation energy. The results on transition strengths brings in an additional sensitive probe to test residual interactions [20]. Sub-barrier CE was also performed on a mixed beam of ^{62}Mn and ^{62}Fe. Here a new transition in ^{62}Mn was found at 418 keV, which has been tentatively associated to a $(2^+, 3^+) \rightarrow 1^+_{g.s.}$ transition. Moreover, the relative positions of the β-decaying 4^+ and 1^+ states in ^{62}Mn were determined for the first time. Population of the 2^+_1 state was observed in ^{62}Fe after CE. The corresponding $B(E2; 2^+_1 \rightarrow 0^+_1)$ value in ^{62}Fe was determined by taking into account also previously measured lifetimes which were obtained with the recoil-distance Doppler-shift method. By combining the complementary lifetime and CE data, the first measurement of the spectroscopic quadrupole moment $Q_s(2^+_1)$ of the first-excited 2^+ state could be made [28].

3.2.2. The case of ^{68}Ni. In ^{68}Ni a small $B(E2; 0^+_1 \rightarrow 2^+_1)$ value was first determined by a CE experiment at intermediate energy at GANIL. The ^{68}Ni beam was produced from the fragmentation of a ^{70}Zn beam with an energy of 65.9 MeV/A [73]. A complementary measurement was performed using CE at the REX-ISOLDE facility employing a beam at 'safe' energies below the Coulomb barrier. The ^{68}Ni beam was accelerated to 2.9 MeV/A and directed onto a ^{108}Pd target. The measured value of $B(E2; 0^+_1 \rightarrow 2^+_1) = 2.8^{+1.2}_{1.0} \cdot 10^2 e^2$ fm^4 is in good agreement with the value measured at intermediate energy confirming the low $0^+_1 \rightarrow 2^+_1$ transition probability [19].

Future safe CE experiments on more neutron-rich nickel isotopes are not hindered by the in-target production using proton-induced fission but by the slow release out of the target matrix and by potential contamination of gallium isobars. In future primary ISOL-target developments will reduced the release time in the seconds range and suppress the gallium contamination in order to extend CE experiments towards the doubly-magic ^{78}Ni nucleus.

3.2.3. Isomeric beams of Cu isotopes. The availability of post-accelerated radioactive beams in combination with isomer-selective resonant laser ionization at ISOLDE opened the way for a new type of investigation, because the laser ionization is able to provide Cu beams of odd-odd nuclei with different nuclear spin [74]. This allowed experiments of the different configurations, present in the same nucleus, through CE. The first low-energy CE measurements were performed with isomeric radioactive beams of odd-odd nuclei ^{68,70}Cu at energies of 2.83 MeV/A. Both beams consisted of long lived $I^\pi = 6^-$ isomers.

The experiments in the neutron-rich Cu isotopes were motivated by the monopole migration, the sudden lowering of the proton $\pi 1f5/2$ orbital with the increased occupancy of the neutron $\nu 1g_{9/2}$ orbital, along the chain of $^{69-73}$Cu nuclei. The energy shift was interpreted as originating from the residual proton–neutron interaction. The isomeric beams were exploited to study the multiplet of states (3^-, 4^-, 5^-, 6^-) arising from the proton–neutron $\pi 2p_{3/2} \otimes \nu 1g_{9/2}$ configuration. The 4^- state of the multiplet was populated via CE and the $B(E2; 6^- \rightarrow 4^-)$ value was determined in $^{69-73}$Cu. The $B(E2; 6^- \rightarrow 4^-)$ value of the $\pi 2p_{3/2} \otimes \nu 1g_{9/2}$ multiplet in ^{70}Cu was determined to be lower, indicating weak polarization effects induced by the extra proton and neutron coupled to ^{68}Ni. However, the results show that the coupling of at least two quasi-particles to ^{68}Ni weakens the stabilization effects of the $N = 40$ subshell and $Z = 28$ shell gaps. A comparison with large-scale shell-model calculations using the ^{56}Ni core shows the importance of the proton excitations across the

$Z = 28$ shell gap to the understanding of the nuclear structure in the neutron-rich nuclei with $N \approx 40$ [17].

Another first-time CE experiment was performed with a ^{70}Cu beam whose intensity was dominated by the 3^- isomeric state allowing the CE of states on top of the $I^\pi = 3^-$ isomer. In addition to the previous results with a $I^\pi = 6^-$ beam in ^{70}Cu, the complementary experiment allowed the study of the multiplet of states (3^-, 4^-, 5^-, 6^-) arising again from the $\pi 2p_{3/2} \otimes \nu 1g_{9/2}$ configuration to be completed. Besides the known γ-ray transition deexciting the 4^- state, a ground-state γ ray of 511 keV was observed and was associated with the 5^- state. This observation established the energy, spin, and parity of the 5^- member of the $\pi 2p_{3/2} \otimes \nu 1g_{9/2}$ multiplet, completing the low-energy level scheme of ^{70}Cu. $B(E2)$ values for all possible $E2$ transitions within the multiplet were determined. Some of the previous $B(E2)$ values were revised, because the new experimental data allowed them to be determined without relying on theoretical assumptions. The experimental results were compared to large-scale shell-model calculations using different valence spaces and different values of the effective residual proton–neutron interaction. The shell-model calculations starting from a ^{56}Ni core reproduced both the absolute $B(E2)$ values and their trend when large effective charges for protons $e_\pi = 1.9e$ and neutrons $e_\nu = 0.9e$ were used. The large polarization of the ^{56}Ni core is explicitly taken into account in a second shell-model calculation in the *fpgd* space starting from a ^{48}Ca core and including the $\nu 2d_{5/2}$ orbital for neutrons. Indeed this calculation reproduces the absolute values and their trend using a standard $0.5e$ polarization charge. From the comparison of the two calculations it seemed necessary to include the $\nu 2d_{5/2}$ orbital. However, when including the $\nu 2d_{5/2}$ orbital, the calculation predicts an enhancement in collectivity in ^{72}Cu which is not observed experimentally [23].

A second series of measurements in Cu isotopes concentrated on the collective properties of the low-lying levels in the four odd ^{67,69,71,73}Cu isotopes. These odd-proton nuclei span the $N = 40$ neutron-subshell and $N = 3$ oscillator-shell closure at ^{68}Ni. The isotopic chain was investigated by CE with radioactive post-accelerated beams at REX-ISOLDE up to 2.99 MeV A^{-1}. In ^{67,69}Cu, low-lying $1/2^-$, $5/2^-$, and $7/2^-$ states were populated. In ^{71,73}Cu, decays from the single-particle-like $5/2^-$ and core-coupled $7/2^-$ levels were identified. Besides these known transitions γ rays of 454 and 135 keV were observed for the first time. Based on a re-analysis of β-decay work and comparison with the systematics, a spin $1/2^-$ was proposed for these excited states. Three $B(E2)$ values for the transitions depopulating low-energy $1/2^-$, $5/2^-$, and $7/2^-$ states were determined in each of the four isotopes. The new low-energy levels at 454 and 135 keV have unexpectedly large $B(E2)$ values. The results indicate a significant change in the structure of the odd Cu isotopes beyond $N = 40$ where single-particle-like and collective levels are suggested to coexist at very low excitation energies.

The increased collectivity could indicate significant deformation, although the position of these levels were foreseen in the vibrational-model based calculations. The results indicate a significant drop in the $B(E2; 5/2^- \rightarrow 3/2^-)$ value that points to a change from a rather collective to a single-particle-like structure for the $5/2^-$ level at $N = 40$ and beyond. The data revealed the presence of both single-particle and collective states at low energy in the neutron-rich Cu nuclei that drop with increasing value of N and lie at approximately the same energy. This behavior illustrates the sensitivity of the transition rates to the details of the wave functions [18].

3.2.4. Neutron-rich Zn isotopes and the N = 50 shell closure. The experimental $B(E2; 2_1^+ \rightarrow 0_1^+)$ values in the Zn isotopic chain show a parabolic behavior towards $N = 40$ similar as the Ni isotopes. However at $N = 40$ (^{70}Zn), the $B(E2; 2_1^+ \rightarrow 0_1^+)$ value suddenly increases. This observation was qualitatively interpreted as the onset of deformation and increased collectivity due to the addition of two protons outside the $Z = 28$ closed shell, the maximum of neutron pairing at $N = 40$ and the presence of the $l = 4$ Nilsson neutron orbital close to the Fermi surface. For a considerable deformation with $\beta \approx 0.23$ (extracted from the $B(E2)$ value), the inclusion of the $1g_{9/2}$ orbital in the valence space is crucial in order to reproduce the increased $B(E2; 0_1^+ \rightarrow 2_1^+)$ value in ^{70}Zn. The more neutron-rich even–even zinc isotopes with two protons outside the $Z = 28$ proton shell and the gradual occupation of neutrons in the $1g_{9/2}$ orbital are ideally suited to study the evolution of the $Z = 28$ shell gap and the stability of the $N = 50$ neutron shell gap near ^{78}Ni.

The radioactive ^{74,76,78,80}Zn isotopes were produced by high-energy proton- and neutron-induced fission of ^{238}U, combined with selective laser ionization and mass separation. The low-energy CE experiments yielded the $B(E2; 2_1^+ \rightarrow 0_1^+)$ values in $^{74-80}$Zn. For ^{74,76}Zn the $B(E2; 4_1^+ \rightarrow 2_1^+)$ values were measured additionally. The 2_1^+ states were established in ^{78,80}Zn. For the first time the $2_1^+ \rightarrow 0_1^+$ transition in ^{80}Zn was observed at 1492 keV. With only two protons outside the $Z = 28$ proton core, ^{80}Zn was the lightest $N = 50$ isotone for which spectroscopic information has been obtained for the first time.

The $B(E2)$ and $E(2_1^+)$ systematics for zinc isotopes and $N = 50$ isotones were compared with large-scale shell-model calculations. The results for the zinc isotopes were accounted for reasonably well by two calculations. The first interaction (SMI) included a large proton effective charge of $e_\pi = 1.9$e and neutrons $e_\nu = 0.9$e. The second empirical residual interaction for the $f_{5/2}p_{3/2}p_{1/2}g_{9/2}$ model space (JJ4B calculations) [75] performs overall very well in the calculation of the $B(E2\downarrow)$ and $E(2_1^+)$ in the $N = 50$ isotonic chain compared to the SMI calculations. No direct evidence was found for an enhanced $Z = 28$ core polarization, but the larger proton effective charge needed in the SMI calculations to describe $N = 50$ isotones with $Z < 40$ indicate a larger proton-core polarization for these isotopes. At this time no evidence appeared for breaking of the $N = 50$ shell gap [16, 21].

3.3. Approaching ^{100}Sn

The isotopes between ^{100}Sn and ^{132}Sn constitute the longest semi-magic chain in the nuclear chart and they have for this reason since long been a testing ground for nuclear models. The purpose of the REX-ISOLDE experiments in the ^{100}Sn region has sofar been to investigate the robustness of the $N = Z = 50$ shell closure using CE. Several isotopes, namely ^{100,102,104}Cd [31], ^{107,109}Sn [33, 34] and ^{106,107,108}In [32, 35], have been studied with measurements on ^{106,108,110}Sn as highlights [29, 30] (see figure 5).

In the experiments on the even ^{100,102,104}Cd isotopes Ekstrom *et al* [31] extracted data for the reduced transition probability, $B(E2; 0_{gs}^+ \rightarrow 2_1^+)$, and the quadrupole moment, $Q(2_1{}^+)$, and developed a maxium likelihood method for the probability distribution of the $(B(E2),Q(2_1{}^+))$ pair. The analysis method, applied for the first time in a radioactive beam experiment, was used to investigate the neutron effective charge in the ^{100}Sn region. The experiment also put a limit on the $B(E2; 0_{gs}^+ \rightarrow 2_1^+)$ in ^{100}Cd. In measurements on ^{106,108}In, Ekstrom *et al* [32] reanalyzed the $\pi g_{9/2}^{-1} \otimes \nu d_{5/2}$ and $\pi g_{9/2}^{-1} \otimes \nu g_{7/2}$ multiplets. They also confirmed the 7^+ spin and parity of the ground state in ^{106}In and concluded that the ordering of the ground state and close lying isomeric state had inverse order compared to shell model predictions in ^{108}In. In experiments on the light odd Sn isotopes, Di Julio *et al* [33, 34] investigated the structure of

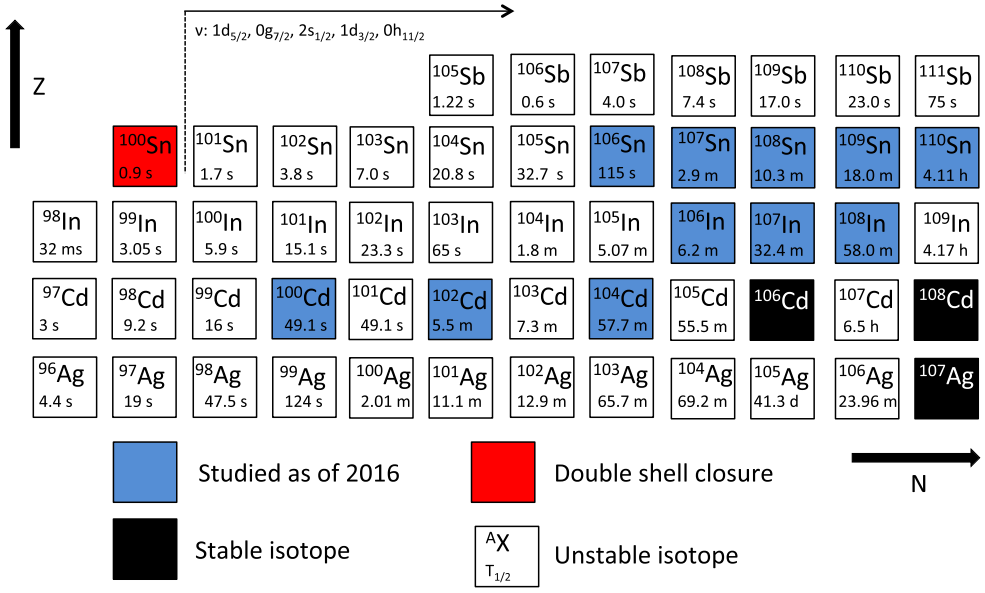

Figure 5. The REX-ISOLDE program in the ^{100}Sn region started in 2003 with preparations for measurements on the light even mass Sn isotopes. These experiments were followed by Coulomb excitation of the even Cd isotopes and later of odd Sn and In isotopes. See text for further discussion.

^{107,109}Sn and put constraints on the single-particle dominated orbits in the odd Sn isotopes. In experiments on ^{106,108,110}Sn Cederkall *et al* [29] and Ekstrom *et al* [30] addressed the strength of the shell closure at ^{100}Sn. The remaining part of this section will expand on this topic.

In the even Sn isotopes the wave function of the lowest excited states is to a large extent built on the $\nu(d_{5/2}, g_{7/2}, s_{1/2}, d_{3/2}, h_{11/2})$ orbits above the $N = 50$ gap. On the neutron deficient side, i.e. for Sn isotopes with a mass number, $A < 112$, the $\nu(d_{5/2}, g_{7/2})$ orbits should dominate if ^{100}Sn is a good shell closure. Potential components e.g. from excitations across the $Z = 50$ gap that would change this picture can be investigated using different methods. The approach used at REX-ISOLDE relies on determining the reduced transitions probabilities from the ground state to the first 2^+ state, the $B(E2; 0^+_{gs} \rightarrow 2^+_1)$, in even Sn isotopes as function of neutron number. The results are then compared to predictions from large scale shell model calculations (LSSM) based on the assumption that ^{100}Sn is doubly magic.

3.3.1. The light even Sn isotopes. When the program started in 2003 there was an indication of a deviation between prediction and experiment in the $B(E2; 0^+_{gs} \rightarrow 2^+_1)$ for ^{112,114}Sn, while the even isotopes from ^{116}Sn to ^{130}Sn were well described by LSSM calculations (see figure 6). In parallel with the preparations at REX-ISOLDE, a complementary experiment, aiming to use a relativistic beam of ^{108}Sn, was also in preparation at GSI. The result from that measurement, which was published in 2005 [76], pointed to a difference between the experimental $B(E2; 0^+_{gs} \rightarrow 2^+_1)$ value and model predictions also for that isotope but it had a large statistical error.

The need to use radioactive ion beams to expand the $B(E2; 0^+_{gs} \rightarrow 2^+_1)$ measurements to neutron deficient Sn isotopes stems from isomerism in the yrast cascade which hampers measurements of the reduced transition probabilities of the first 2^+ state using fusion evaporation reactions and traditional Doppler shift methods. This isomerism arises from the

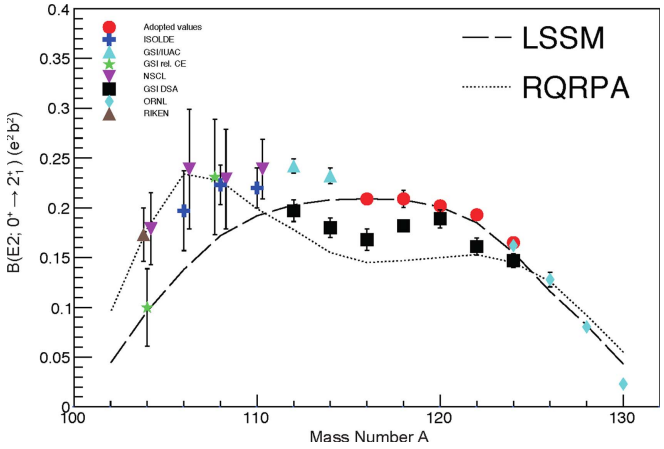

Figure 6. Summary of reduced transition probabilities, $B(E2; 0^+_{gs} \rightarrow 2^+_1)$, for the even Sn isotopes. The REX-ISOLDE results [29, 30] are indicated with blue crosses and the results from high-energy CE from GSI [76, 79], NSCL [80] and RIKEN [81] are given by green stars, and pink and brown triangles, respectively. The results from a typical LSSM calculation [76] and an RQRPA calculation [82] are shown with long and short dashed lines. The LSSM calculation, based on a ^{100}Sn core with the $\nu(d_{5/2}, g_{7/2}, s_{1/2}, d_{3/2}, h_{11/2})$ model reproduces the adopted values (given by red circles) [83] as well as the data from ORNL for $^{124-130}$Sn [84], while a clear deviation occurs below ^{116}Sn. An expansion of the model space to include excitations of protons in the $g_{9/2}$ orbit across the $Z = 50$ gap tends to increase the transition strength towards midshell but gives only small shifts in the maximum [76]. In a rather recent development the reduced transition probabilities for the stable isotopes $^{112-124}$Sn have also been revisited (black squares) using Doppler shift attenuation methods [85]. See text for further discussion.

relatively small energy difference between the yrast 4^+ and 6^+ states, where the 6^+ state is the highest-spin state that can be constructed by breaking a pair in the $\nu(d_{5/2}, g_{7/2})$ dominated 0^+ ground state. In addition, the use of CE at safe energies has the advantage of producing results that can be compared to measurements of the stable isotopes in the chain without the risk of introducing method dependent systematic differences.

Different target materials were investigated as the first step of the program. Data from ORNL and GSI [77] showed that molecular beams of SnS from a Ce_2S_x target could be advantageous in order to suppress isobaric contaminants using the molecular sideband. This approach should also increase the intensity for beams of short-lived Sn isotopes due to the relatively short release times for the SnS molecule. Desorption times two orders of magnitude shorter for SnS compared to atomic Sn has been reported the literature [77]. Target tests were therefore performed to benchmark the molecular SnS beam against laser ionization using an LaC_x target. The intensity of the laser ionized beam proved to be considerably higher than for the molecular sideband. Although significant amounts of In isobars, from surface ionization, could be expected due to the relatively low ionization potential of In (5.78 eV), it was concluded that laser ionization could be employed for Sn beams down to mass number 106, under the condition that the ionization efficiency was monitored during the experiment to determine beam purity. The lifetimes of ^{110}Sn, ^{108}Sn, ^{106}Sn are 4.1 h, 10.3 m and 115 s, respectively and the release time of Sn from a LaC_x matrix at ca 2000 degrees is 100 s or longer [77]. Sn beams extracted from an LaC_x target using laser ionization are therefore, with a typical PS booster supercycle, almost continuous. In contrast, the contaminant In is released within seconds. Yield measurements show that ca 85% of the In isotopes with half lifes above

5 s exit the target before they decay [78]. The amount of contaminant could therefore be reduced by using a supercycle with consecutive pulses followed by several empty pulses. This method gave a beam purity of ∼90%, 60% and 30% for ^{110}Sn, ^{108}Sn and ^{106}Sn, respectively.

Four runs were performed using post-accelerated beams of ^{110,108,106}Sn at an energy of 2.8 MeV A^{-1}. The trapping efficiency was 40%–60% while the charge breeding, to the 26^+, 27^+ and 30^+ charge states used in the different experiments, had typical efficiencies of 8%–10%. The transmission through the post-accelerator varied between 60% and 80% thus yielding a typical total transmission of ca 5% from production to secondary target. The intensities at the secondary target were 10^6 p s^{-1} for ^{110,108}Sn and 10^5 p s^{-1} for ^{106}Sn. For ^{110}Sn the intensity of the proton driver was reduced to 7×10^{12} p/pulse compared to the nominal 3×10^{13} p/pulse in order not to overwhelm the detector system. Following bombardment of targets of ^{58}Ni with typical thickness of 2 mg cm^{-2}, γ-ray yields of 588(24), 994(38) and 133(14) counts were obtained for the $2_1^+ \rightarrow 0_{gs}^+$ transition in respectively ^{110}Sn, ^{108}Sn and ^{106}Sn. The corresponding $B(E2; 0_{gs}^+ \rightarrow 2_1^+)$ values were determined to be 0.220(22) e^2b^2, 0.222(19) e^2b^2 and 0.195(39) e^2b^2.

These results, which were pioneering measurements of the reduced transition probabilites in the ^{100}Sn region, remain unique. They have considerably better precision than the earlier measurement on ^{108}Sn and therefore stand as the first systematic confirmation that current LSSM calculations cannot properly account for the trend of the $B(E2; 0_{gs}^+ \rightarrow 2_1^+)$ values in the Sn chain. The measurements at REX-ISOLDE were followed by measurements using high-energy CE at NSCL(^{104,106,108,110}Sn), GSI (^{104}Sn), and at RIKEN (^{104}Sn). Taken together these measurements confirm a stronger excitation strength to the first 2^+ state than expected from LSSM calculations (see figure 6) although some deviation can be seen for the GSI measurement of ^{104}Sn, which was limited by statistics.

Several calculations were performed as part of the interpretation of the REX-ISOLDE experiments in the ^{100}Sn region. From the theoretical standpoint the Sn chain has been a good example of the seniority scheme [86] exhibiting almost constant 2_1^+ energies and an increasing trend of $B(E2; 0_{gs}^+ \rightarrow 2_1^+)$ values from the $N = 82$ shell closure towards midshell. Such simple relations are not valid per default in general seniority, although Morales *et al* [87] have shown that simple trends can be reproduced under certain conditions. Studies of the overlap of the seniority-two wave function with the first 2^+ state in the shell model, e.g. by Sandulescu *et al* [88], give overlaps ranging from ca 93% in ^{104}Sn down to ca 42% in ^{112}Sn. This indicates that a trunctation scheme based on seniority-two states is inadequate for heavier isotopes in the Sn chain.

The general dependence on neutron number sketched above is nevertheless reproduced in many LSSM calculations. A set of illustrative calculations performed by Banu *et al* [76], and later expanded on by Ekstrom *et al* [30], are good benchmarks for LSSM calculations in the light Sn isotopes and describe the current limitations. The first of these using a ^{100}Sn core is presented as a typical result of an LSSM calculation in figure 6. It is in excellent agreement with the adopted values for the stable isotopes and the ORNL data for the heavy unstable isotopes, while it underestimates the transition strengths below ^{114}Sn. To investigate the effects of proton excitations across the $Z = 50$ gap the same authors performed a calculation including up to $4p$–$4h$ proton core excitations. This calculation, which was performed with seniority truncation, increases the transition strength midshell but does not reproduce the strength for the lower mass numbers. Ekstrom *et al* [30] performed additional calculations, using a ^{100}Sn core, and included charge symmetry breaking as well as charge independence breaking. Their calculation shows a first sign of an asymmetric trend of the reduced transition probabilities with respect to midshell but does still not produce the enhancement for the lower mass numbers. Additional work has also been done by Ansari [82] using RQRPA (see RQRPA label in figure 6). Although the prediction

underestimates the transition strength in the heavy isotopes a clear increase in strength, reproducing the general behavior of the experimental data, can be seen for the lighter isotopes. This prediction prompted remeasurements of the $B(E2; 0^+_{gs} \rightarrow 2^+_1)$ in the midshell isotopes using Doppler shift attenuation methods at GSI and ANU. Interestingly, those results show statistically significant deviations from the adopted values for the same isotopes. This situation still remains and new measurements are considered.

Finally, the basic input parameters to any shell-model calculation are the two body matrix elements (TBME) and the single particle energies (SPE) with respect to the core. As the structure of ^{101}Sn has still not been established in experiment, calculations continue to rely on SPEs and TBMEs extracted from excitation spectra of neighboring atomic nuclei and, for TBMEs, on derivations based on microscopic descriptions of the nucleon–nucleon interaction. The microscopic approach to TBMEs is attractive as it provides a way to test microscopic descriptions of the nucleon–nucleon interaction in few-particle nuclei [89]. However, as the SPEs in the Sn region are largely unknown [90, 91] one aim for the future program at HIE-ISOLDE is therefore to perform transfer reactions to the single-particle dominated states in the odd Sn isotopes to cast further light on this topic.

3.4. Evolution of quadrupole collectivity away from closed shells

Bauer *et al* [44] and Stegmann *et al* [45] investigated the evolution of quadrupole collectivity for the $N = 80$ isotones, by measuring the $B(E2; 2^+_1 \rightarrow 0^+_1)$ in ^{140}Nd and ^{142}Sm respectively. While the value of $B(E2)$ for $^{140}_{60}$Nd has the expected dependence on $N_\pi N_\nu$ (whereas a dip is observed [92] for $^{138}_{58}$Ce corresponding to the $\pi(g_{7/2})$ subshell closure at $Z = 58$), the value for $^{142}_{62}$Sm deviates significantly from the $N_\pi N_\nu$ behavior, reflecting the impact of the $\pi(1g_{7/2}2d_{5/2})$ subshell closure at $Z = 64$.

Grahn *et al* [93] measured the $B(E2; 2^+_1 \rightarrow 0^+_1)$ in ^{206}Po and ^{208,210}Rn. They observed that contributions from collective excitations are present in these nuclei when moving away from the $N = 126$ closed shell, although they have been proposed to lie in, or at the boundary of the region where the seniority scheme should persist.

4. Shape coexistence

Shape coexistence occurs at low excitation energy in which near degenerate states appear that have different shapes. The distinctive character of shape coexistence lies in the subtle interplay between two opposing trends: shell and subshell closures that invoke a stabilizing effect leading to sphericity, and residual interactions between protons and neutrons outside closed shells that drive the nucleus to deformation. The latter arise from multiparticle multi-hole excitations above the proton shell closures that interact with neutrons, which fill high-j intruder orbits. The significant gain in nuclear binding energy arising from the pairing and the proton–neutron correlation energy decreases the excitation energy of the corresponding 0^+ state in even–even nuclei so that it appears at low excitation energy or even becomes the ground state. For recent experimental reviews, see Görgen [94], Görgen and Korten [95] and Wrzosek-Lipska and Gaffney [96]. Several regions where shape coexistence occurs have been studied at REX-ISOLDE using MINIBALL.

4.1. $N \approx Z$ nuclei near ^{72}Kr

Following the observation of low-lying 0^+ states in the light Kr isotopes Clément *et al* [97] carried out pioneering experiments, in this case using the SPIRAL facility at GANIL, to accelerate

^{74}Kr and ^{76}Kr isotopes, enabling the CE yields of several states in these nuclei to be measured. By combining the Coulex data with nuclear lifetime date, enough matrix elements could be measured accurately to enable the shape of the ground-state band and the band built on the excited 0^+ state to be determined in a model-independent way using rotational invariant products of the $E2$ operator. This provided firm experimental proof that the ground states of both nuclei are prolate, while the excited 0^+ state bands are triaxial. Using the REX-ISOLDE facility Hurst *et al* [37] measured the Coulex yield of the lowest 2^+ state in ^{70}Se. In order to remove isobaric contaminants, the ^{70}Se was extracted from the ZrO_2 production target in the form of a complex molecule ($^{70}Se^{12}C^{16}O^+$) that was broken up in REXEBIS, so that a two-stage A/q selection could be applied. By combining the Coulex yield with the available lifetime measurement a prolate shape for the 2^+ state was deduced. A subsequent re-measurement of the 2^+ lifetime found it to be much longer [98], so that only the hypothesis of an oblate shape is consistent with both Coulex yield and lifetime, in agreement with theoretical expectations.

4.2. Neutron rich Kr, Sr, Zr near $N = 60$

The sudden onset of deformation observed for neutron rich Zr and Sr nuclei at $N = 60$ belongs to the most dramatic shape changes in the nuclear chart. This shape transition is accompanied by the appearance of low-lying 0^+ states that, for $N < 60$, can be interpreted as a deformed configuration that becomes the ground state at $N = 60$, while the spherical ground-state configuration of the isotopes with $N < 60$ becomes nonyrast for those with $N \geqslant 60$ (see [95] and references therein). The systematics of the excitation energies of the 2_1^+ states and $B(E2; 0_1^+ \rightarrow 2_1^+)$ for even–even nuclei around $N = 60$ are given in figure 7. The shape transition is explained (see [38] and references therein) as a consequence of the strongly interacting proton and neutron Nilsson orbitals. For the neutrons, the downsloping $\nu 1/2^-[550]$ and the $\nu 3/2^-[541]$ orbitals, both resulting from the spherical $\nu h_{11/2}$ orbital, drive the deformation. Meanwhile, the extruder $\nu 9/2^+[404]$ orbital stabilizes the deformation at a saturation level of about $\beta \approx 0.4$. On the other hand, for the protons, the downsloping $\pi 1/2^+[440]$ and $\pi 3/2^+[431]$ orbitals, originating from the spherical $\pi g_{9/2}$ orbital, are fully occupied at $Z = 38$ and $Z = 40$, again at a deformation $\beta \approx 0.4$. These proton intruder orbitals have a large spatial overlap with the neutron intruder orbitals, creating a minimum in the binding energy at $\beta \approx 0.4$. At the neutron number $N = 60$ this deformed configuration is favored over the spherical one and deformation sets in rapidly.

Clément *et al* [42, 99] measured the spectroscopic quadrupole moments of low-lying states in ^{96}Sr and ^{98}Sr and reduced transition probabilities between bands, using CE. The ^{96}Sr beam was produced by injecting CF_4 gas into the target ion source and extracting $^{96}Sr^{19}F$ molecules. The otherwise dominant ^{96}Rb contamination was removed by setting the mass separator to the molecular mass at $A = 115$. The molecules were subsequently broken up in the charge breeder. In the case of ^{98}Sr, with a half-life of 653 ms, the ^{98}Rb ($T_{\frac{1}{2}} = 102$ ms) contaminant was suppressed by keeping the $A = 98$ ions sufficiently long in the REXTRAP for most of the Rb to decay to Sr, resulting in an 80% pure ^{98}Sr beam. The measurements of the spectroscopic quadrupole moments of excited 2^+ states established shape coexistence of highly deformed prolate and spherical configurations in ^{98}Sr. A comparison of $B(E2)$ values and the spectroscopic quadrupole moments of the 2_1^+ state in ^{96}Sr and the 2_2^+ state in ^{98}Sr underlined their similarity and establishes the shape inversion at $N = 60$. In this work the interpretation of measured reduced $E2$ matrix elements using a phenomenological two-band mixing model substantiates the weak mixing between prolate and spherical configurations in the wave functions of the 0^+ states in ^{98}Sr, in spite of their proximity in energy.

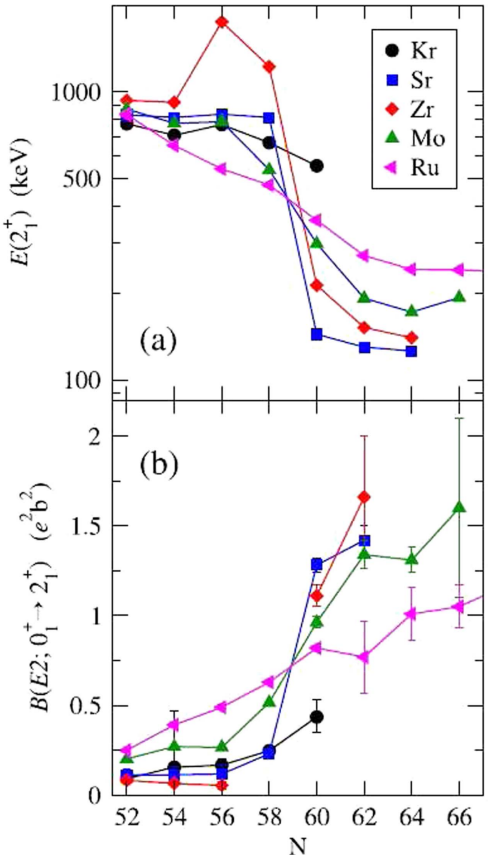

Figure 7. Excitation energies of the 2_1^+ states and $B(E2; 0_1^+ \rightarrow 2_1^+)$ for even–even nuclei around $N = 60$. Reproduced from [95]. © IOP Publishing Ltd. All rights reserved.

Albers *et al* [38, 39] measured the transition $E2$ matrix element between the ground and the first 2^+ state, and the diagonal matrix element of the 2^+ state, for ^{92,94,96}Kr, using CE. While the quadrupole moment increases significantly between $N = 56$ and $N = 60$, no sudden onset of deformation was observed.

Sotty *et al* [40] reported Coulomb-excitation measurements on the neutron-rich isotopes $^{97}Rb_{60}$ and $^{99}Rb_{62}$ produced as radioactive beams. The challenge for these experiments was the short beam half-lives, 169 ms and 54 ms respectively for ^{97}Rb and ^{99}Rb, that required short trapping and breeding times in REXTRAP and REXEBIS in order to minimize in-flight decay. The excited states in these odd-A nuclei, that form rotational bands built on the ground state, were observed for the first time. The results provide clear-cut evidence for enhanced quadrupole collectivity of the ^{97,99}Rb nuclei and firmly identify the deformation-driving configuration of the odd proton. Detailed information on the $M1$ transition strengths in ^{97}Rb provided concrete experimental evidence for the $\pi g_{9/2}[431]3/2^+$ Nilsson-configuration assignment.

4.3. Neutron-deficient Hg, Po, Rn region

CE experiments to study electromagnetic properties of radioactive even–even Hg isotopes were performed with 2.85 MeV/nucleon mercury beams from REX-ISOLDE. These represented the first time that such heavy beams were accelerated using the facility, paving the way

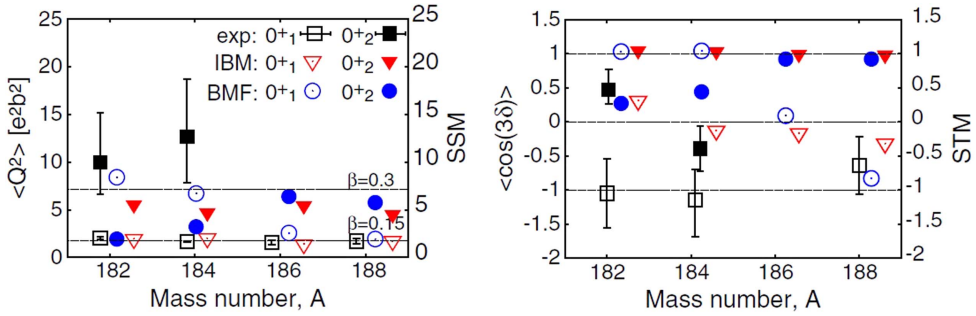

Figure 8. The sum of squared $E2$ matrix elements (SSM) and sum of triple $E2$ matrix element products (STM) values of the 0_1^+ (open symbols) and 0_2^+ (full symbols) for Hg isotopes [46], compared with various theoretical models (for details, see [46]). Within the quadrupole collective models the values of SSM and STM can be related to the quadrupole invariants $\langle Q^2 \rangle$ and $\langle \cos(3\delta) \rangle$ representing the overall deformation and the axial asymmetry, respectively. Reprinted figure with permission from [46], Copyright 2014 by the American Physical Society.

for other studies of nuclei in this mass region and heavy nuclei in the octupole actinide mass region. For these heavy nuclei internal conversion plays an important role in the analysis and information from the K x-ray yield, enhanced over that expected from atomic processes arising from beam-target collisions [100], and β-decay studies (see [46] and references therein) were used to determine the $E0$ component of the 2_2^+ to 2_1^+ transition as well as the population of the 0_2^+ state. In addition, independent lifetime measurements were made of excited states in ^{182,184,186}Hg (see [46] and references therein). From the combined data set, magnitudes and relative signs of the reduced $E2$ matrix elements that couple the ground state and low-lying excited states in $^{182-188}$Hg were extracted. Information on the deformation of the ground and the first excited 0^+ states was deduced using the quadrupole sum rules approach, see figure 8. The results showed [46] that the ground state is slightly deformed and of oblate nature, while a larger deformation for the excited 0^+ state was noted in ^{182,184}Hg. In contrast to that observed in the Sr, Zr isotopes with $N = 60$, the co-existing bands in the light mercury isotopes were shown to strongly mix. This accounts for the almost constant excitation energy observed for the first 2^+ state in $^{182-188}$Hg.

Coulomb excitation studies of ^{196,198,200,202}Po [47] and ^{202,204}Rn [48] were also carried out. For the polonium isotopes the observed behavior of the deformation of the ground state is consistent with charge radii measurements [101] that indicate the onset of significant deformation occurring for $A < 199$. Although there is a paucity of data for the 0_2^+ and 2_2^+ states in these nuclei, calculations using a two-level mixing model for the polonium isotopes hint at the spin-independent mixing of a more spherical structure with a weakly deformed oblate structure. For the radon isotopes matrix elements were determined for the $2_1^+ \rightarrow 0_1^+$ transitions and (for $A = 202$ only) the $4_1^+ \rightarrow 2_1^+$ and $2_2^+ \rightarrow 2_1^+$ transitions. The precision from this experiment is not sufficient to distinguish between oblate-, prolate-, and spherical-like charge distributions.

5. Octupole deformed structures in nuclei with $A \approx 220$

Strong octupole correlations leading to pear shapes can arise for certain proton and neutron numbers Z and N. When both proton and neutron numbers have these values, such as for

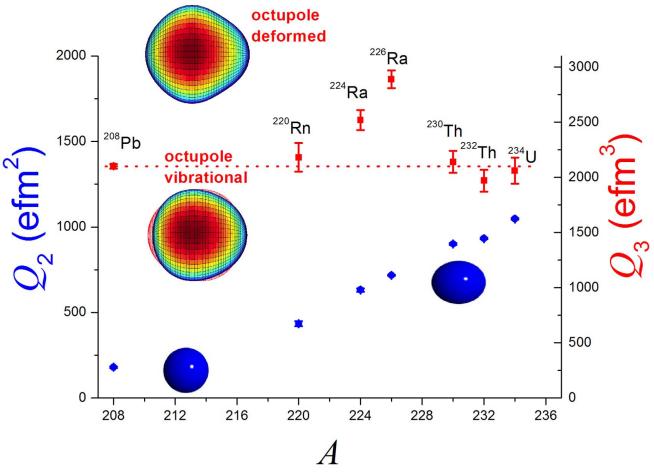

Figure 9. The systematics of measured $E2$ (circles) and $E3$ (squares) intrinsic moments Q_λ for $\lambda \rightarrow 0$ transitions in nuclei with $A > 200$. The moments are related to the transition matrix elements using the expression given in the caption of figure 3 in [49]. Reproduced from [102]. © IOP Publishing Ltd. All rights reserved.

$Z \sim 56$, $N \sim 88$ and $Z \sim 88$, $N \sim 134$ we expect the best evidence for reflection asymmetry. While the bulk of the evidence comes from the behavior of energy levels for even–even nuclei, the $E3$ moment is an observable that is insensitive to single-particle effects and provides the best measure of enhanced octupole correlations, and for deformed nuclei can be related to the intrinsic octupole deformation parameters (for review, see [102]). Until recently, $E3$ transition moments had been determined for only one nucleus in the $Z \approx 88$, $N \approx 134$ region, ^{226}Ra [103]. In this case the radioisotope is sufficiently long-lived to produce a macroscopic target sample. The technique has now been extended by the use of accelerated radioactive beams from REX-ISOLDE [49]. In order to study octupole correlations in nuclei in the $Z \approx 88$, $N \approx 134$ region, ^{220}Rn and ^{224}Ra ions were produced by spallation in a thick uranium carbide target. The ions were post-accelerated in REX-ISOLDE to an energy of 2.8MeV per nucleon and bombarded various secondary targets. In sub-Coulomb reactions the $E2$ and $E3$ transition moments dominate the excitation process allowing these moments to be determined from measurement of the cross-sections of the states. Figure 9 compares the experimental values of Q_λ derived from the matrix elements connecting the lowest states for nuclei near $Z = 88$ and $N = 134$ measured by CE. It is striking that while the $E2$ moment increases by a factor of 6 between ^{208}Pb and ^{234}U, the $E3$ moment changes by only 50% in the entire mass region. Nevertheless, the larger Q_3 values for ^{224}Ra and ^{226}Ra indicate an enhancement in octupole collectivity that is consistent with an onset of octupole deformation in this mass region. On the other hand, ^{220}Rn has similar octupole strength to ^{208}Pb, ^{230,232}Th and ^{234}U, consistent with it being an octupole vibrator. More details on the comparison with theoretical models and the relevance of these measurements to searches for CP-violating static electric dipole moments in atoms can be found in [102].

6. Summary and outlook

High-resolution γ-ray spectroscopy has been established at ISOLDE for nuclear-structure studies with reaccelerated radioactive ion beams provided by the REX-ISOLDE facility. The

MINIBALL spectrometer has been used in numerous experiments exploiting Coulomb excitation, at safe energies, and transfer reactions with beams of energies up to 3 MeV A^{-1}. The physics cases have been investigated across a wide range of the Segré chart ranging from neutron-rich magnesium isotopes up to heavy radium isotopes. The studies range from shell model investigations of exotic nuclei at or near closed shells, and measurements of nuclear deformation and collectivity that have elucidated the various shapes and geometrical symmetries of the nucleus.

In the future the HIE-ISOLDE facility will allow the in-beam spectroscopy program to proceed with higher secondary-beam intensity, higher beam energy and better beam quality. The previous REX-ISOLDE linac will be replaced in stages by a superconducting linac. Two superconducting cavities were put into operation and first CE experiments with an increased beam energy of 5.5 MeV A^{-1} were performed in late 2016. The new facility will enlarge the scope of the ongoing investigations by multi-step CE for all radioactive beams available at ISOLDE. Moreover, future transfer experiments will benefit from the higher energies and will allow an extended range for optimizing the Q-value matching condition. The final HIE-ISOLDE linac will reach an energy of 10 MeV A^{-1}. This will enable transfer reaction studies employing heavy mass beams up to masses around $A = 200$. Finally, the MINIBALL spectrometer will be augmented with new instrumentation such as the SPEDE conversion electron spectrometer [104], an upgraded version of Si detectors for the T-REX array, Anti-Compton BGO suppression shields for the HPGe triple-cluster detectors and a new digital electronics and data acquisition system in order to enlarge the detection capabilities.

Acknowledgments

The authors would like to acknowledge financial support from the following agencies: the German BMBF under contracts 06-K167, 06-KY205I, 06-OK668, 06-OK862I, 06-OK958, 06-KY9136I, 05P12PKFNE, 05P15PKCIA, the European Community under TMR contract TMR ERBFMRX CT97-0123, the Swedish Research Council under contracts VR-2003-2737, 2009-3939, 2010-5942, 2013-4178, and the UK Science and Technology Facilities Council.

References

[1] Habs D *et al* 1997 *Z. Phys.* A **358** 161–2
[2] Habs D *et al* 1997 *Prog. Part. Nucl. Phys.* **38** 111–26
[3] Ames F *et al* 2005 *Nucl. Instrum. Methods Phys. Res.* A **538** 17–32
[4] Wenander F 2002 *Nucl. Phys.* A **701** 528–36
[5] Wenander F 2010 *J. Instrum.* **5** C10004
[6] Habs D *et al* 1998 *Nucl. Instrum. Methods* B **139** 128–35
[7] Habs D *et al* 2000 *Hyperfine Interact.* **129** 43–66
[8] Kester O *et al* 2003 *Nucl. Instrum. Methods Phys. Res.* B **204** 20–30
[9] Habs D *et al* 1994 Radioactive beam experiments at ISOLDE: Coulomb excitation and neutron transfer reactions of exotic nuclei *Proposal to the ISOLDE Committee* CERN/ISC 94-25 ISC/P68
[10] Scheit H *et al* 2004 *Nucl. Phys.* A **746** 96–102
[11] Niedermaier O *et al* 2005 *Phys. Rev. Lett.* **94** 172501
[12] Wimmer K *et al* 2010 *Phys. Rev. Lett.* **105** 252501
[13] Seidlitz M *et al* 2011 *Phys. Lett.* B **700** 181–6
[14] Seidlitz M *et al* 2014 *Phys. Rev.* C **89** 024309
[15] Siebeck B *et al* 2015 *Phys. Rev.* C **91** 014311
[16] van de Walle J *et al* 2007 *Phys. Rev. Lett.* **99** 142501

[17] Stefanescu I *et al* 2007 *Phys. Rev. Lett.* **98** 122701
[18] Stefanescu I *et al* 2008 *Phys. Rev. Lett.* **100** 112502
[19] Bree N *et al* 2008 *Phys. Rev.* C **78** 047301
[20] van de Walle J *et al* 2009 *Eur. Phys. J.* A **42** 401
[21] van de Walle J *et al* 2009 *Phys. Rev.* C **79** 014309
[22] Diriken J *et al* 2010 *Phys. Rev.* C **82** 064309
[23] Rapisarda E *et al* 2011 *Phys. Rev.* C **84** 064323
[24] Illana A *et al* 2014 *Phys. Rev.* C **89** 054316
[25] Diriken J *et al* 2014 *Phys. Lett.* B **736** 533–8
[26] Orlandi R *et al* 2015 *Phys. Lett.* B **740** 298–302
[27] Diriken J *et al* 2015 *Phys. Rev.* C **91** 054321
[28] Gaffney L P *et al* 2015 *Eur. Phys. J.* A **51** 136
[29] Cederkäll J *et al* 2007 *Phys. Rev. Lett.* **98** 172501
[30] Ekström A *et al* 2008 *Phys. Rev. Lett.* **101** 012502
[31] Ekström A *et al* 2009 *Phys. Rev.* C **80** 054302
[32] Ekström A *et al* 2010 *Eur. Phys. J.* A **44** 355–61
[33] DiJulio D D *et al* 2012 *Phys. Rev.* C **86** 031302
[34] DiJulio D D *et al* 2012 *Eur. Phys. J.* A **48** 105
[35] DiJulio D D *et al* 2013 *Phys. Rev.* C **87** 017301
[36] Ilieva S *et al* 2014 *Phys. Rev.* C **89** 014313
[37] Hurst A M *et al* 2007 *Phys. Rev. Lett.* **98** 072501
[38] Albers M *et al* 2012 *Phys. Rev. Lett.* **108** 062701
[39] Albers M *et al* 2013 *Nucl. Phys.* A **899** 1–28
[40] Sotty C *et al* 2015 *Phys. Rev. Lett.* **115** 172501
[41] Bottoni S *et al* 2015 *Phys. Rev.* C **92** 024322
[42] Clément E *et al* 2016 *Phys. Rev. Lett.* **116** 022701
[43] Bauer C *et al* 2012 *Phys. Rev.* C **86** 034310
[44] Bauer C *et al* 2013 *Phys. Rev.* C **88** 021302
[45] Stegmann R *et al* 2015 *Phys. Rev.* C **91** 054326
[46] Bree N *et al* 2014 *Phys. Rev. Lett.* **112** 162701
[47] Kesteloot N *et al* 2015 *Phys. Rev.* C **92** 054301
[48] Gaffney L P *et al* 2015 *Phys. Rev.* C **91** 064313
[49] Gaffney L P *et al* 2013 *Nature* **497** 199–204
[50] van Duppen P and Riisager K 2011 *J. Phys. G: Nucl. Part. Phys.* **38** 024005
[51] Warr N *et al* 2013 *Eur. Phys. J.* A **49** 40
[52] Eberth J *et al* 1997 *Prog. Part. Nucl. Phys.* **38** 29–37
[53] Eberth J *et al* 2001 *Prog. Part. Nucl. Phys.* **46** 389–98
[54] Warr N *et al* 2004 *Eur. Phys. J.* A **20** 65–6
[55] Ostrowski A *et al* 2002 *Nucl. Instrum. Methods Phys. Res.* A **480** 448–55
[56] Bildstein V *et al* 2007 *Prog. Part. Nucl. Phys.* **59** 386–8
[57] Bildstein V *et al* 2012 *Eur. Phys. J.* A **48** 85
[58] Motobayashi T *et al* 1995 *Phys. Lett.* B **346** 9–14
[59] Pritychenko B *et al* 1999 *Phys. Lett.* B **461** 322–8
[60] Church J A *et al* 2005 *Phys. Rev.* C **72** 054320
[61] Chisté V *et al* 2001 *Phys. Lett.* B **514** 233–9
[62] Michimasa S *et al* 2014 *Phys. Rev.* C **89** 054307
[63] Niedermaier O 2005 Low-energy Coulomb excitation of the neutron-rich Mg isotopes ^{30}Mg and ^{32}Mg *Doctoral Dissertation* University of Heidelberg
[64] Mach H *et al* 2005 *J. Phys. G: Nucl. Part. Phys.* **31** S1421
[65] Wildenthal B 1984 *Prog. Part. Nucl. Phys.* **11** 5–51
[66] Utsuno Y *et al* 1999 *Phys. Rev.* C **60** 054315
[67] Rodríguez-Guzmán R, Egido J and Robledo L 2002 *Nucl. Phys.* A **709** 201–35
[68] Neyens G *et al* 2005 *Phys. Rev. Lett.* **94** 022501
[69] Hurst A *et al* 2009 *Phys. Lett.* B **674** 168–71
[70] Pritychenko B V *et al* 2002 *Phys. Rev.* C **66** 024325
[71] Ettenauer S *et al* 2008 *Phys. Rev.* C **78** 017302
[72] Utsuno Y *et al* 2004 *Phys. Rev.* C **70** 044307
[73] Sorlin O *et al* 2002 *Phys. Rev. Lett.* **88** 092501

[74] Köster U *et al* 2000 *Nucl. Instrum. Methods* B **160** 528 –535
[75] Lisetskiy A F *et al* 2004 *Phys. Rev.* C **70** 044314
[76] Banu A *et al* 2005 *Phys. Rev.* C **72** 061305
[77] Köster U *et al* 2008 *Nucl. Instrum. Methods* B **266** 4229–39
[78] Köster U 2002 *Eur. Phys. J.* A **15** 255–63
[79] Guastalla G *et al* 2013 *Phys. Rev. Lett.* **110** 172501
[80] Vaman C *et al* 2007 *Phys. Rev. Lett.* **99** 162501
[81] Doornenbal P *et al* 2014 *Phys. Rev.* C **90** 061302
[82] Ansari A 2005 *Phys. Lett.* B **623** 37–42
[83] Raman S, Nestor C and Tikkanen P 2001 *At. Data Nucl. Data Tables* **78** 1–128
[84] Radford D *et al* 2004 *Nucl. Phys.* A **746** 83–9
[85] Jungclaus A *et al* 2011 *Phys. Lett.* B **695** 110–4
[86] Racah G 1942 *Phys. Rev.* **62** 438–62
[87] Morales I O, Isacker P V and Talmi I 2011 *Phys. Lett.* B **703** 606–8
[88] Sandulescu N *et al* 1997 *Phys. Rev.* C **55** 2708–10
[89] Hjorth-Jensen M, Kuo T T and Osnes E 1995 *Phys. Rep.* **261** 125–270
[90] Seweryniak D *et al* 2007 *Phys. Rev. Lett.* **99** 022504
[91] Darby I G *et al* 2010 *Phys. Rev. Lett.* **105** 162502
[92] Rainovski G *et al* 2006 *Phys. Rev. Lett.* **96** 122501
[93] Grahn T *et al* 2016 *Eur. Phys. J.* A **52** 340
[94] Görgen A 2010 *J. Phys. G: Nucl. Part. Phys.* **37** 103101
[95] Görgen A and Korten W 2016 *J. Phys. G: Nucl. Part. Phys.* **43** 024002
[96] Wrzosek-Lipska K and Gaffney L P 2016 *J. Phys. G: Nucl. Part. Phys.* **43** 024012
[97] Clément E *et al* 2007 *Phys. Rev.* C **75** 054313
[98] Ljungvall J *et al* 2008 *Phys. Rev. Lett.* **100** 102502
[99] Clément E *et al* 2016 *Phys. Rev.* C **94** 054326
[100] Bree N *et al* 2015 *Nucl. Instrum. Methods* B **360** 97–102
[101] Seliverstov M *et al* 2013 *Phys. Lett.* B **719** 362–6
[102] Butler P A 2016 *J. Phys. G: Nucl. Part. Phys.* **43** 073002
[103] Wollersheim H *et al* 1993 *Nucl. Phys.* A **556** 261–80
[104] Papadakis P *et al* 2015 *JPS Conf. Proc.* **6** 030023